estec

European Space Research
and Technology Centre
Keplerlaan 1
2200 AG Noordwijk
The Netherlands
Tel. (31) 71 565 8332
www.esa.int

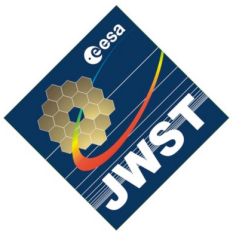

NIRSpec Performance Report
NPR-2013-006 / ESA-JWST-RP-19656

Authors: Guido De Marchi & Giovanna Giardino

Date of Issue: 24 May 2013
Version: 1

Calibration of the GWA position sensors – Part III – Target acquisition accuracy

ABSTRACT

We have investigated the performance of the position sensors of the imaging mirror installed on the NIRSpec grating wheel assembly (GWA), using observations collected through the micro shutter array (MSA) during the second NIRSpec flight model ground calibration campaign. We confirm the previously reported tight relationship between the sensor's readings and the offset along the dispersion direction, across the entire field of view, with a residual scatter of less than 2.5 mas (RMS). As regards the cross-dispersion direction, we find that in most cases (85% of the trials) there is no systematic offset, with a repositioning accuracy better than 2.5 mas (RMS). The quoted accuracy also includes uncertainties on the geometrical transformations between the plane of the detector and that of the micro shutter array (MSA) and on their temporal stability, as well as on the uniformity of the MSA and detector metrology. These results are relevant for the NIRSpec target acquisition requirements, and we show that all components in the error budget pertaining to the NIRSpec opto-mechanical train and to its stability are met with ample margin.

1 INTRODUCTION

The NIRSpec grating wheel assembly (GWA) contains eight selectable optical elements, providing dispersion into spectra as well as imaging of the field of view (FOV) for target acquisition purposes. Any rotational non-repeatability of the GWA will result in a small shift of the image or spectrum at the detector plane. For good science performance, these shifts have to be minimised, accurately measured and corrected for if too large. To this aim, a set of magneto-resistive position and tilt sensors are installed on the GWA, to provide information on the actual position of the optical elements when they are used.

For a description of the GWA sensors and an analysis of their performance during the first NIRSpec flight model ground calibration campaign see De Marchi (2012a) and De

Marchi et al. (2012b). In those papers, images and spectra collected through the NIRSpec fixed slits and integral field unit are used to characterise the performance of the position sensors in the dispersion direction for those observing modes. In this work, we extend the study to the entire NIRSpec FOV, using observations collected through the micro shutter array (MSA). Since the specific interest in this paper is to quantify the uncertainties affecting the target acquisition process, the analysis focuses on observations collected in imaging mode, through the mirror installed on the GWA. A companion paper (Alves de Oliveira & De Marchi 2013) addresses the performance of the dispersive elements, namely the gratings and the prism.

The structure of this report is organised as follows. In Section 2 we describe the data and the analysis that was applied to them, while the results are presented in Section 3. Besides characterising the properties of the GWA, the purpose of this work is to demonstrate compliance with the NIRSpec-specific target acquisition requirements contained in the NIRSpec Target Acquisition Requirements Document (Böker 2008) and listed in Table 1. Therefore, Section 4 is devoted to comparing our findings with the target acquisition requirements and compliance is shown. Furthermore, we discuss there compliance with the higher-level requirements for target acquisition contained in the NIRSpec Functional Requirements Document (Smith 2008). Finally, the most important conclusions of this work are summarised in Section 5.

Requirement	Topic	Compliant	Method
TA8 (SRD R-204)	Internal image motion due to fore optics	yes	measured
TA9 (SRD R-94)	Image motion of collimator/camera optics	yes	measured
TA10 (SRD R-177)	Sky to MSA transformation calibration	yes	derived
TA10 (SRD R-178)	MSA to FPA transformation calibration	yes	measured
TA10 (SRD R-179)	Sky to FPA transformation calibration	yes	derived
TA11 (SRD R-230)	Knowledge of imaging mirror orientation	yes	measured
TA12 (SRD R-220)	Knowledge of filter-induced image shift	yes	derived
FRD NSFR-37	Accuracy of targets placement	yes	derived

Table 1. List of requirements covered in this report. Compliance is verified by direct measurement or derived from the analysis of those measurements. Requirements contained in the NIRSpec Target Acquisition Requirements Document (Böker 2008) are indicated by the corresponding TA number, but for each of them the table also provides the original requirement (SRD R- number) contained in the NIRSpec System Requirements Document (Jensen 2013). The last row shows the specific target acquisition requirement contained in the Functional Requirements Document (Smith 2008) that we verify in this work.

2 OBSERVATIONS AND DATA ANALYSIS

The data used for this work were obtained during cycle 1 of the second NIRSpec flight model calibration campaign that took place at IAGB, Ottobrunn, Germany from 2012 December to 2013 February (Gnata 2013). We used observations obtained through the MSA configured in a “checkerboard” pattern, in which one micro-shutter every four is open, both in the dispersion and in the cross-dispersion direction. An example of one such configuration is shown in Figure 1, illustrating a detail of MSA quadrant 3, while the complete list of exposures taken with this MSA configuration is provided in Table 2. Following the procedures developed by Giardino (2012), from these exposures one can

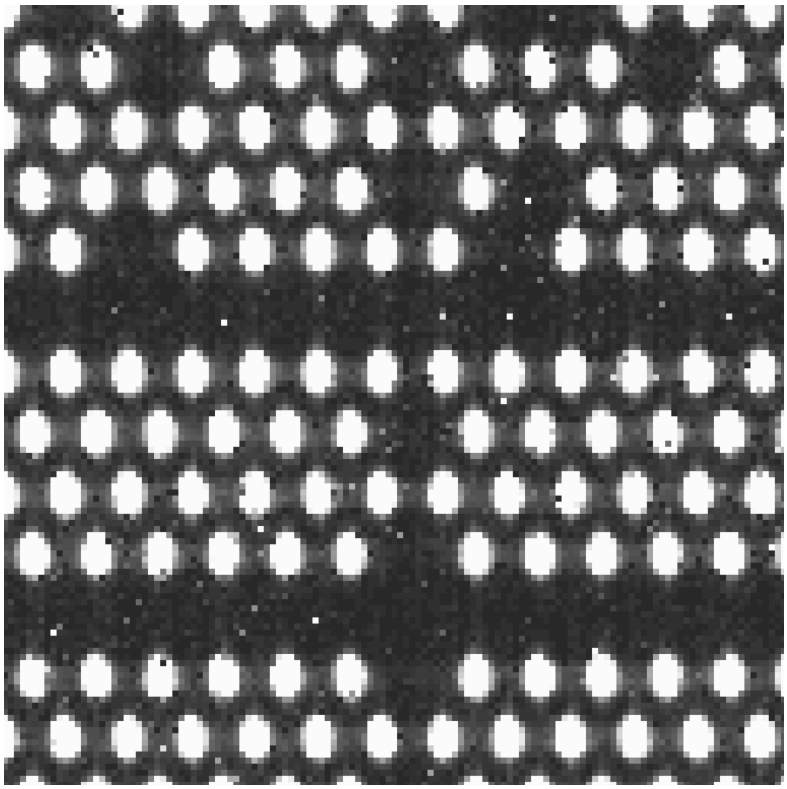

Figure 1. Image showing a portion of quadrant Q3 in a "checkerboard" configuration. One micro-shutter every four is commanded open in both directions. Rows and columns of permanently closed micro-shutters as well as individual failed-closed micro-shutters are visible.

derive the mapping between MSA shutters and their projection onto the focal plane array (FPA), i.e. the detector, in pixel coordinates. The output of this procedure consists of two linear transformations (FPA-to-MSA and MSA-to-FPA) and of two sets of 5^{th}-order polynomial coefficients describing the corresponding distortions. Using these transformations, it is possible to predict the pixel position of the centre of each micro-shutter projected on the detector. The only implicit assumption made in deriving these transformations is that the geometry of the MSA and FPA is regular, i.e. that all micro-shutters are rectangular and have the same size and pitch everywhere across the MSA and that the pixel grid of the detector is the same across the entire FPA (information on the MSA and FPA metrology can be found in, respectively, Schwinger 2010 and Redman 2010). As we will conclude in Section 4, if any deviation from uniformity is present, it must be very small and as such it does not affect our conclusions.

All exposures listed in Table 2 were obtained with the same NIRSpec configuration, i.e. with the same MSA configuration, the same internal calibration source, the same filter and the same GWA optical element, namely the mirror. In principle, they should all provide the same set of transformation coefficients. However, due to the limited mechanical angular reproducibility of the GWA mechanism, the nominal centre of a given micro-shutter will have slightly different pixel coordinates in every exposure, since the GWA position has changed between the exposures. Therefore, each exposure in Table 2 corresponds to a different set of transformation coefficients for the MSA-to-FPA mapping and, of course, for the reverse FPA-to-MSA transformations.

NID	GWA conf.	FWA conf.	Calib. source	GWA Temp.	Date	Time
7781	MIRROR	OPAQUE	TEST	39.52	2013-01-10	07:41:16
7967	MIRROR	OPAQUE	TEST	39.53	2013-01-11	05:10:16
7978	MIRROR	OPAQUE	TEST	39.53	2013-01-11	06:44:36
7989	MIRROR	OPAQUE	TEST	39.53	2013-01-11	08:10:18
8394	MIRROR	OPAQUE	TEST	39.45	2013-01-14	04:39:51
8479	MIRROR	OPAQUE	TEST	39.54	2013-01-14	14:24:53
9067	MIRROR	OPAQUE	TEST	39.83	2013-01-16	10:02:17
9098	MIRROR	OPAQUE	TEST	39.54	2013-01-16	17:16:26
9561	MIRROR	OPAQUE	TEST	39.57	2013-01-18	21:01:13
10002	MIRROR	OPAQUE	TEST	39.56	2013-01-20	14:22:05
10403	MIRROR	OPAQUE	TEST	39.54	2013-01-22	15:30:41
10725	MIRROR	OPAQUE	TEST	39.57	2013-01-24	09:32:10
11146	MIRROR	OPAQUE	TEST	39.57	2013-01-25	22:09:55
11567	MIRROR	OPAQUE	TEST	39.59	2013-01-27	10:30:00
11988	MIRROR	OPAQUE	TEST	39.58	2013-01-29	00:31:37
12198	MIRROR	OPAQUE	TEST	39.53	2013-01-29	19:00:16
12830	MIRROR	OPAQUE	TEST	39.43	2013-01-31	23:41:21
13225	MIRROR	OPAQUE	TEST	39.56	2013-02-03	11:42:53
13267	MIRROR	OPAQUE	TEST	39.64	2013-02-03	15:23:46
13285	MIRROR	OPAQUE	TEST	39.97	2013-02-04	00:41:51

Table 2. List of the exposures used in this work. For each observation we list the entry number (NID), the GWA and FWA configurations, the calibration source, the GWA temperature (K), the date and the time (UT).

Therefore, we can use the transformations corresponding to each exposure to probe the pixel offsets caused by the limited repeatability of the GWA in both the dispersion and cross-dispersion directions. Furthermore, we can characterise the performance of the magneto-resistive position and tilt sensors at the mirror and calibrate their response by deriving correlations between detector pixel offsets and corresponding differences in the sensors readings.

The first step in this calibration is characterising the intrinsic uncertainties inherent in the MSA-to-FPA transformations. For this purpose, we have followed the procedures developed by Giardino (2012) but instead of considering all open micro-shutters in the "checkerboard" pattern to derive the transformation coefficients we considered only half of them (one every two in both the dispersion and cross-dispersion direction) and used the obtained coefficients to predict the expected pixel position of the remaining half. We found in this way residuals of 0.004 pixel (rms) or 0.4 mas on the detector, thereby providing the accuracy and confirming the robustness of the transformations. Since each individual observation involves no GWA reconfigurations, the quoted residuals provide a direct measure of the intrinsic uncertainty inherent in the transformations.

Using the MSA-to-FPA transformations, it is possible to derive the pixel coordinates corresponding to the nominal centre of any micro-shutter in each exposure. Thus, pixel offsets between the position of the same micro-shutter in different exposures can be used to probe simultaneously the effects of the GWA repositioning accuracy and the accuracy of the MSA-to-FPA transformations, since each exposure corresponds to a different set of transformation coefficients. In order to probe these effects across the entire FOV, we have selected 16 micro-shutters evenly distributed over the face of each quadrant and have

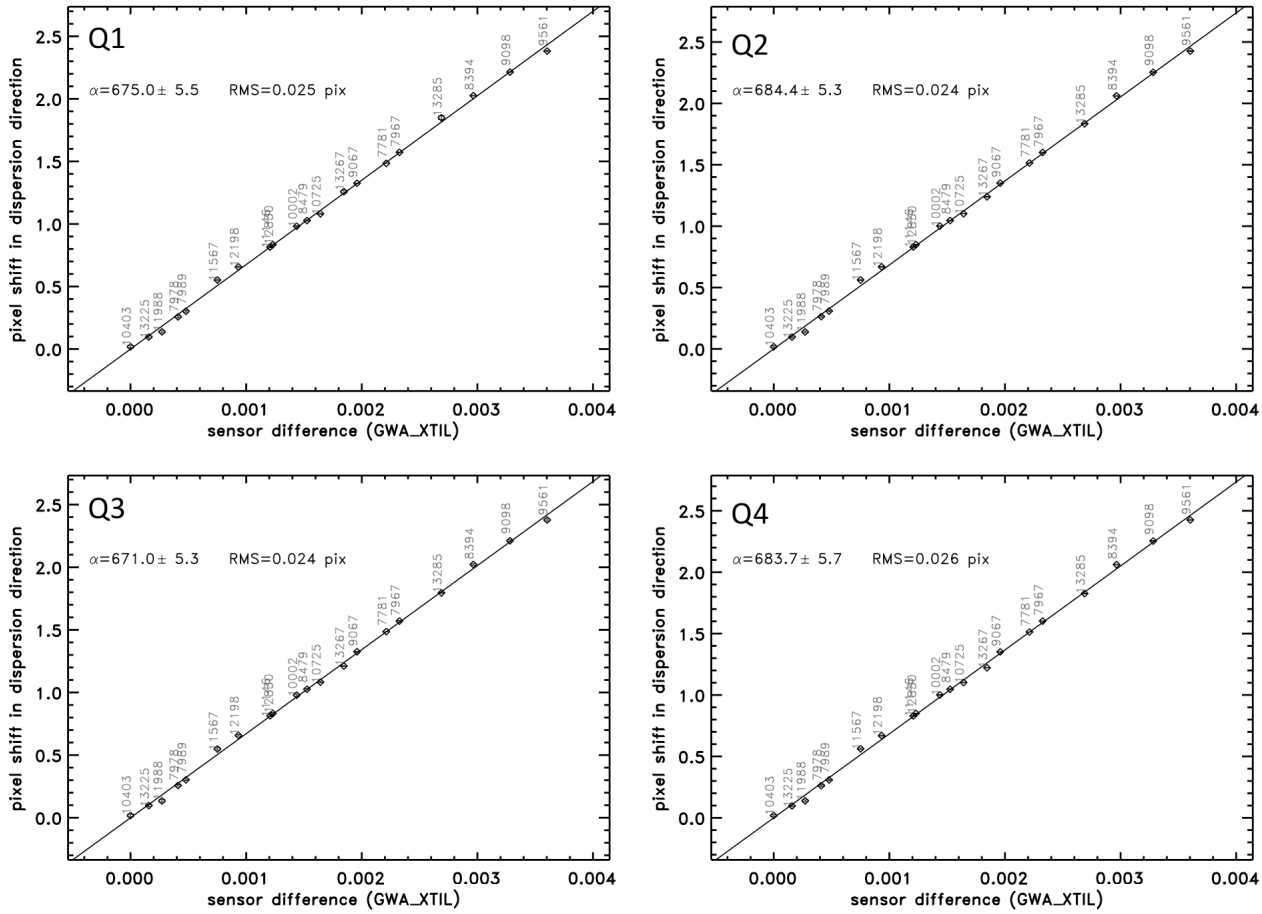

Figure 2. Relative pixel shift measured along the dispersion direction as a function of the readings of the GWA position sensor (GWA_XTIL). The four MSA quadrants are shown separately, as indicated, but they are all consistent with the same (α), within the quoted fit uncertainties. Each observation is identified by the corresponding entry number in the exposures database.

derived the pixel position of their geometrical centres in each of the 20 exposures listed in Table 2. Taking the first of the observations as a reference, we have calculated the pixel offsets for each of these micro-shutters, both in the dispersion and cross-dispersion directions, and have compared them with the readings of the position sensors installed on the GWA. We have experimented with a smaller (9) and larger (25) number of micro-shutters in each quadrant, without finding any systematic differences in the results, as discussed in the following section.

3 RESULTS

The pixel offsets along the dispersion direction are shown in Figure 2 as a function of the differences in the sensor readings. There are various ways in which the sensors can be polled to derive the actual reading (see De Marchi 2012a and 2012b for details on the various telemetry keywords for the GWA sensors) and here we use the most accurate of the GWA sensor readings, corresponding to the telemetry keyword GWA_XTIL. The dots indicate the average offset measured for the 16 micro-shutters in the same image, while the error bars show the corresponding scatter (1 σ), although they are often too small to be

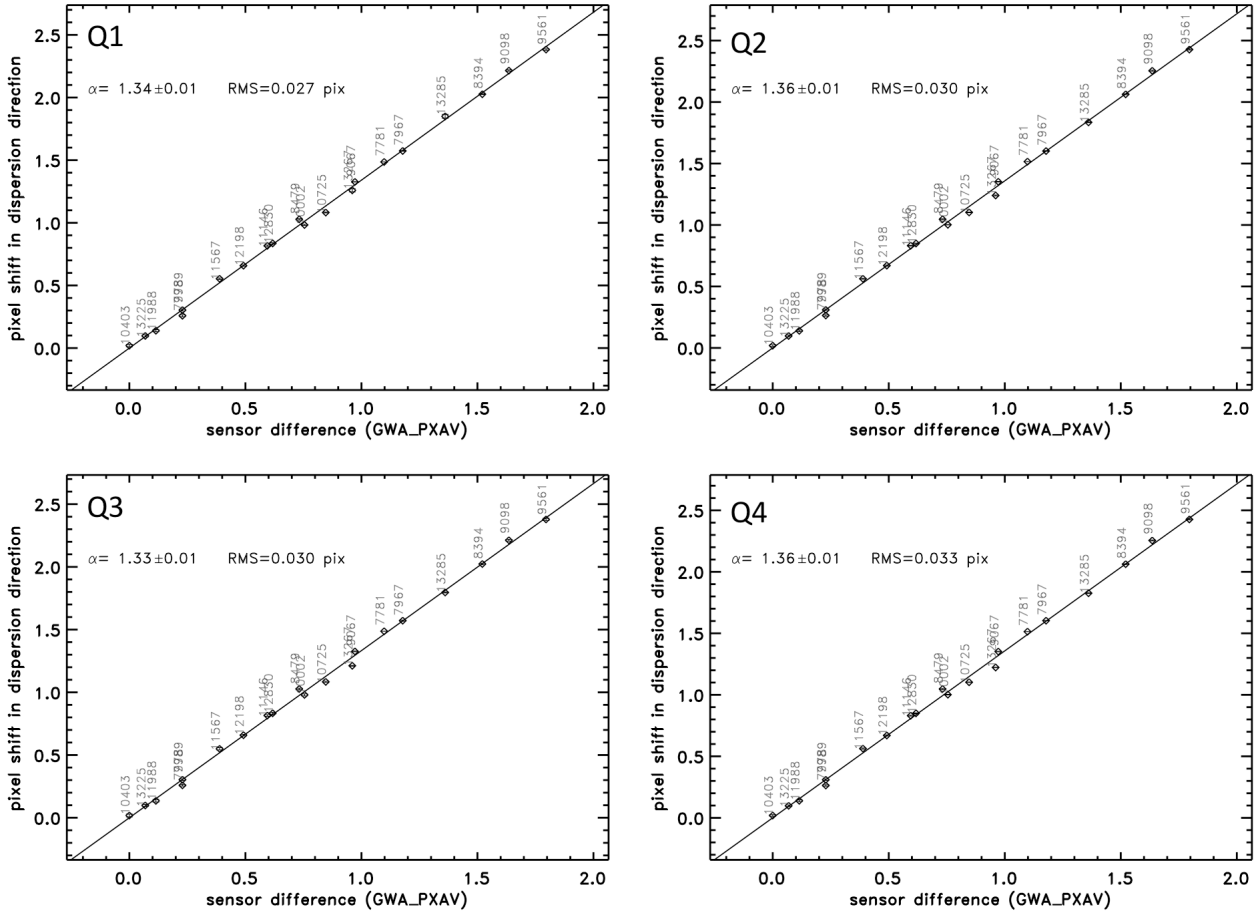

Figure 3. Same as Figure 2, but for a different GWA sensor reading (GWA_PXAV).

seen. The four panels are for the four MSA quadrants, as indicated, and the labels next to each data point correspond to the observation ID listed in Table 2. A linear relation of the type $\Delta X = \alpha \times \Delta V$, corresponding to the solid lines, offers an excellent fit to the data, where ΔX is the pixel offset, ΔV the difference in the voltage readings and α the slope. The values of α and of the corresponding 1 σ uncertainty are given in each panel. Within the uncertainties, all quadrants are compatible with the same slope. If all data points are considered together, regardless of the quadrants to which they belong, the best fitting slope is found to be α = 678.6 with a 1 σ uncertainty of 5.2, in excellent agreement with the individual fits. The residual of the fit is 0.025 pixel (rms) or 2.5 mas. Note that, even though the slope is known to depend on the GWA temperature (De Marchi 2012b), no temperature dependence is found in the data, owing to the very stable temperature during these observations (see Table 2).

The correlation remains very tight if the pixel offsets are plotted against the other telemetry keyword providing the GWA sensor readings, namely GWA_PXAV, which is derived by polling the voltage of the sensor bridge 25 times instead of 256 as in the case of GWA_XTIL (see De Marchi 2012a for details). In both cases, the voltage readings are averaged together and corrected for offsets (as well as for gain differences when it comes to GWA_XTIL), but using GWA_PXAV has the operational advantage of a considerably

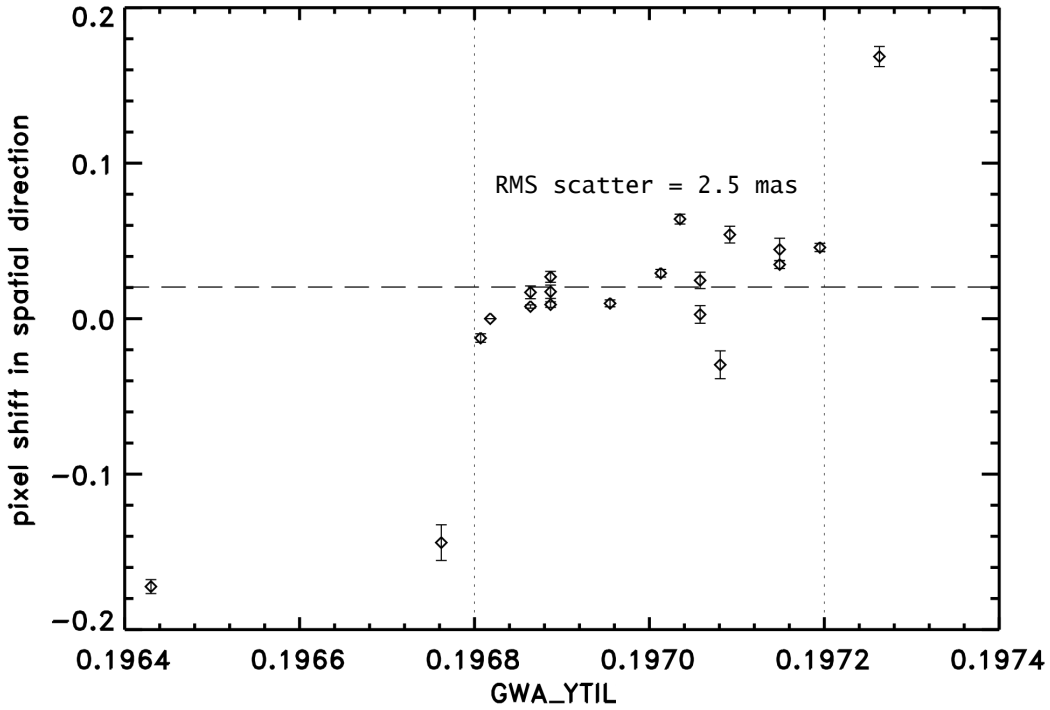

Figure 4. Relative pixel shift measured along the cross-dispersion (spatial) direction as a function of the readings of the GWA position sensor (GWA_YTIL). The actual readings are shown in the figure, rather than the differences with respect to the reference exposure as in previous figures.

shorter execution time. In Figure 3 we show the pixel offsets in the dispersion direction as a function of the differences between the GWA_PXAV values. A linear dependence of the type $\Delta X = \alpha \times \Delta V$, shown by the solid lines, gives once again an excellent fit to theobservations, with residuals of order 3.0 mas (rms). Note that the values of the slope α are different from those shown in Figure 2 because of the different voltage scale (the GWA_PXAV values are not corrected for gain differences). As regards the offsets in the dispersion direction, we can therefore conclude that they can be accurately predicted and corrected for to within 2.5 mas on the basis of the GWA position sensor readings, if we use the GWA_XTIL telemetry keyword, or 3.0 mas if the GWA_PXAV telemetry keywords is used instead.

The offsets in the cross-dispersion (spatial) direction are shown in Figure 4 as a function of the actual values of the GWA_YTIL telemetry keyword. All four quadrants are combined together, since as in the case of the dispersion direction there are no systematic differences between quadrants. The pixel offsets are at least an order of magnitude smaller than those seen in the dispersion direction, indicating a much better repeatability in the repositioning of the GWA. Also the differences in sensor readings are more contained than those in the dispersion direction, at least a factor of five smaller. The average shift in the cross-dispersion direction is 0.01 pixel (dashed line), with a standard deviation of 0.07 pixel. If we apply a standard 2.5 σ clipping procedure, by iteratively discarding all data points departing from the average by more than 2.5 times the standard deviation, only points inside the vertical dotted lines in Figure 4 are retained, corresponding to 85% of the original sample (17 out of 20 points). Their distribution is consistent with no dependence of the cross-dispersion shifts on the sensor's readings, with a residual uncertainty of 0.024 pixel (rms) or 2.4 mas.

For the remaining 15% of the observations, namely those outside the dotted lines, the typical standard deviation is 0.15 pixel or 15 mas. In principle, we could proceed as for the case of the offsets in the dispersion direction and derive a correction based on a linear fit of the type $\Delta Y = \beta \times \Delta V$, where ΔY is the pixel offset, ΔV the difference in the voltage readings and β the slope. The best linear fit, with a slope $\beta = 302.1$, would leave residuals of 0.041 pixel (rms) or 4.1 mas, thereby fully complying with the target acquisition requirements, as discussed in Section 4. However, we believe that the scatter apparent in Figure 4 is simply witnessing random fluctuations in the sensor readings, which, as we will show in Section 4, have no effect on the accuracy or efficiency of target acquisition. These fluctuations only affect a small fraction of the observations (15%) and, therefore, we conclude that it is neither necessary nor worthwhile to account for them when processing the data. This conclusion is based on the fact that, as discussed in Jakobsen (2005), the dispersion direction is the direction of primary scientific concern. Even in the worst-case scenario, affecting only 15% of the observations, an uncertainty of 15 mas in the cross-dispersion direction represents 3.9% of the size of the ~380 mas tall micro-shutter acceptance zone for Band II observations at 2.4 μm (Jakobsen 2005). This value is smaller than the allocated error in the dispersion direction of 4.5% (i.e. 5 mas for an acceptance zone ~110 mas wide) and, therefore, does not represent the leading cause of uncertainty.

A corollary result of this analysis is that the MSA-to-FPA and FPA-to-MSA distortion solutions work equally well and leave equally small residuals for all quadrants, and that all measured offsets are solid, i.e. they reflect a bulk motion as expected. This means that, for the target acquisition process and pipeline calibration, the same set of transformations can be applied to all objects across the entire NIRSpec FOV.

4 CONSEQUENCES FOR TARGET ACQUISITION

The NIRSpec target acquisition concept is presented in Jakobsen (2004a), while the impact of the MSA shutters is extensively discussed in Jakobsen (2004b). In particular, the latter report offers an analytical study of the distortion caused by the opaque grid of the MSA on the determination of the centroids of the reference stars. An evaluation of the total accuracy with which a target of known coordinates can be placed within a preselected 200 mas wide micro-shutter is provided in Jakobsen (2005), and an even more detailed characterisation of the target acquisition error budget is given in Böker (2008). In the following, we will assume that the reader is familiar with the NIRSpec target acquisition procedure, as described in detail in the papers above, and in particular with the complications introduced by the finite repeatability of the GWA mirror. In this work, we are concerned with quantifying, to the extent possible, the contribution of the limited GWA repeatability to the total target acquisition error.

As discussed in Jakobsen (2005), limited GWA repeatability predominantly affects the accuracy of the target acquisition in the dispersion direction, across the narrow dimension of the micro-shutters, which is also the direction of primary scientific concern. The precision required of target acquisition is dictated by the photometric calibration accuracy that is desired for NIRSpec observations (Gnata 2005; Jakobsen 2005). In order to guarantee that any slit losses occurring at the MSA can be properly calibrated, science targets must be placed within their respective micro-shutters with an accuracy of better

than 10% of the size of the shutter. The most stringent requirement is for the positioning along the dispersion direction, so the accuracy must be better than 10% of the 200 mas wide shutter, or 20 mas, as discussed in the NIRSpec Target Acquisition Requirements (Böker 2008). The corresponding accuracy in the cross-dispersion direction, although not discussed in that work, is 45 mas, i.e. 10% of the 450 mas tall shutter. We will show in the following full compliance with these requirements. The requirements levied on target acquisition in the NIRSpec Functional Requirement Document (Smith 2008) are somewhat more stringent, imposing an accuracy of 12.5 mas both in the dispersion and cross-dispersion directions, albeit with the use of up to 20 reference stars, instead of 5 as assumed in the NIRSpec Target Acquisition Requirements (Böker 2008). We will show in the following full compliance with these most stringent requirements, but we note here that there is no rationale for requiring the same accuracy in both the dispersion and cross-dispersion direction, as clarified in Jakobsen (2005) and Böker (2008), since the micro shutters are 2.5 times taller than they are wide.

4.1 Compliance with the System Requirements Document

A graphical representation of the error budget for the NIRSpec target acquisition accuracy is shown in Figure 5, taken from Böker (2008) and from Jakobsen (2005) in its original form. The blue boxes outline the backbone flow of the budget and represent requirements for the observational approach, for the observatory and for in-orbit operations in general, and as such they can only be verified during the commissioning phase. Conversely, the yellow and red boxes indicate the requirements levied on hardware provided, respectively, by ESA and NASA and can already be partly characterised at this stage. In the following we will address and characterise the individual contributions to the error budget that are associated with ESA-provided hardware, showing that there is full compliance with ample margin.

An obvious contribution to the total error budget in Figure 5 is the calibration of the imaging mirror (see box 12, corresponding to req. TA11 and R-230 in Table 1), which we have shown in Section 3 to deliver an accuracy of 2.5 mas, and as such it falls comfortably within the allocated 6.0 mas. In fact, we will show in the following that the intrinsic accuracy must be better than 2.5 mas, since the measurements discussed in Section 3 are also affected by the accuracy of the direct and inverse coordinate transformations between the FPA and the MSA planes. As for the cross-dispersion direction, the accuracy is typically the same (2.5 mas), although it could reach 4.1 mas in extreme cases, as explained in Section 3. In all instances, it is well within the allocated budget.

A good accuracy of the filter correction (see box 11; req. TA12 and R-220 in Table 1) is also needed, in order to compensate for possible systematic offsets between the positions of the same source observed through different filters (e.g. the filter used for target acquisition and the one for the specific band of interest). In this case, the uncertainty allocated to this correction in the error budget is 1 mas, and indeed the currently available data (see Gnata 2013) indicate bulk shifts of less than 1 mas for all filters, except for the F140X – CLEAR and F140X – F170LP pairs. For the latter, the bulk shifts are found to be, respectively, 1.8 mas and 2.1 mas, with a typical 1 σ uncertainty of 0.3 mas (Gnata et al. 2013). Therefore, for all pairs but the latter two no correction is necessary, while for the F140X – CLEAR and

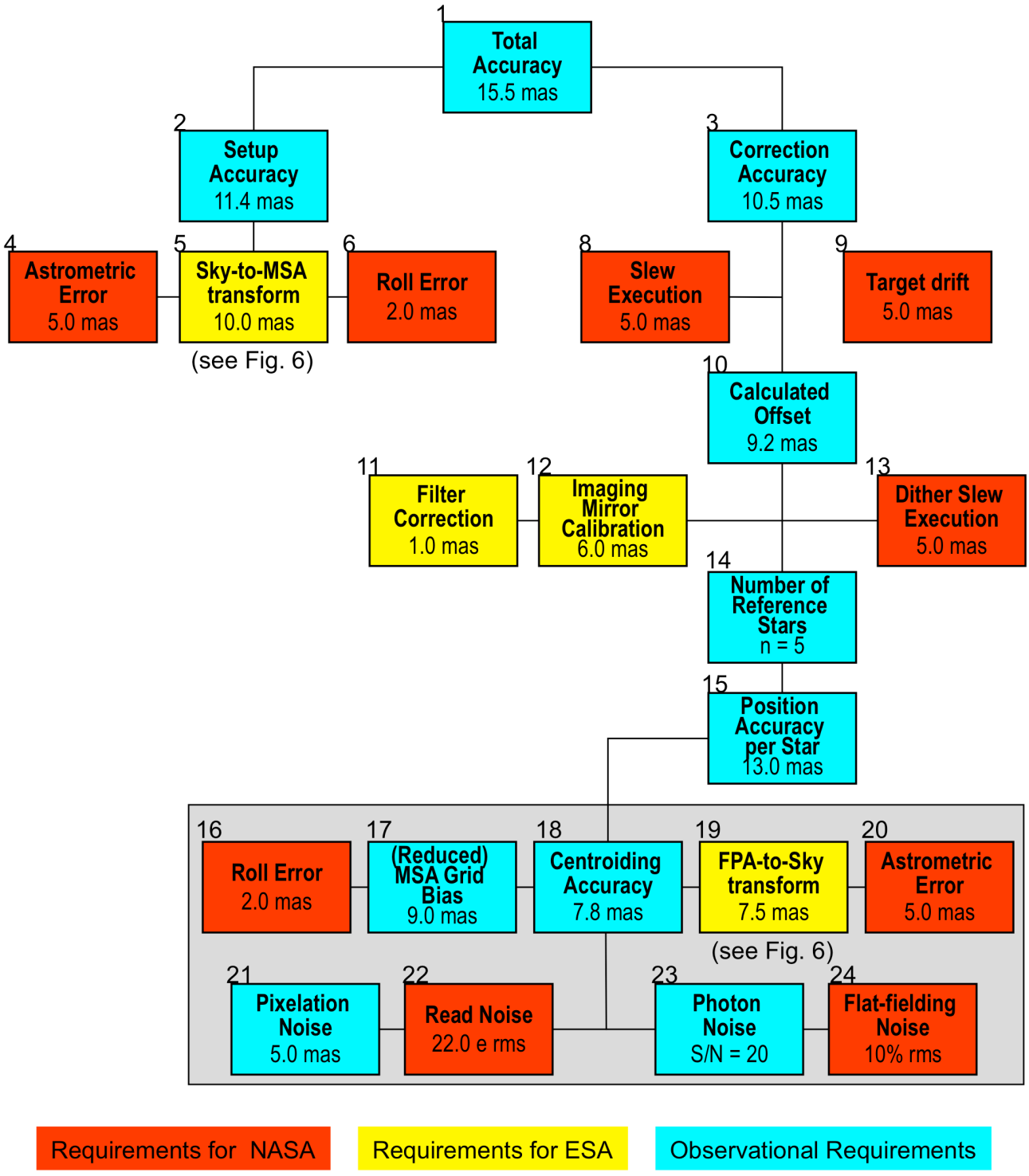

Figure 5. Graphical representation of the error budget for the NIRSpec target acquisition (from Böker 2008). Each box gives the allocated uncertainty. Different colours are used for different type of requirements.

F140X – F170LP pairs a correction should be applied. However, if we make the most conservative assumption that no correction is applied and take 2.5 mas as the maximum uncertainty for any filter pair, the overall uncertainty stemming from the combination of boxes 11 and 12 would not exceed 3.5 mas. This value is considerably smaller than the combined 6.1 mas (rms) allocated for the two components together.

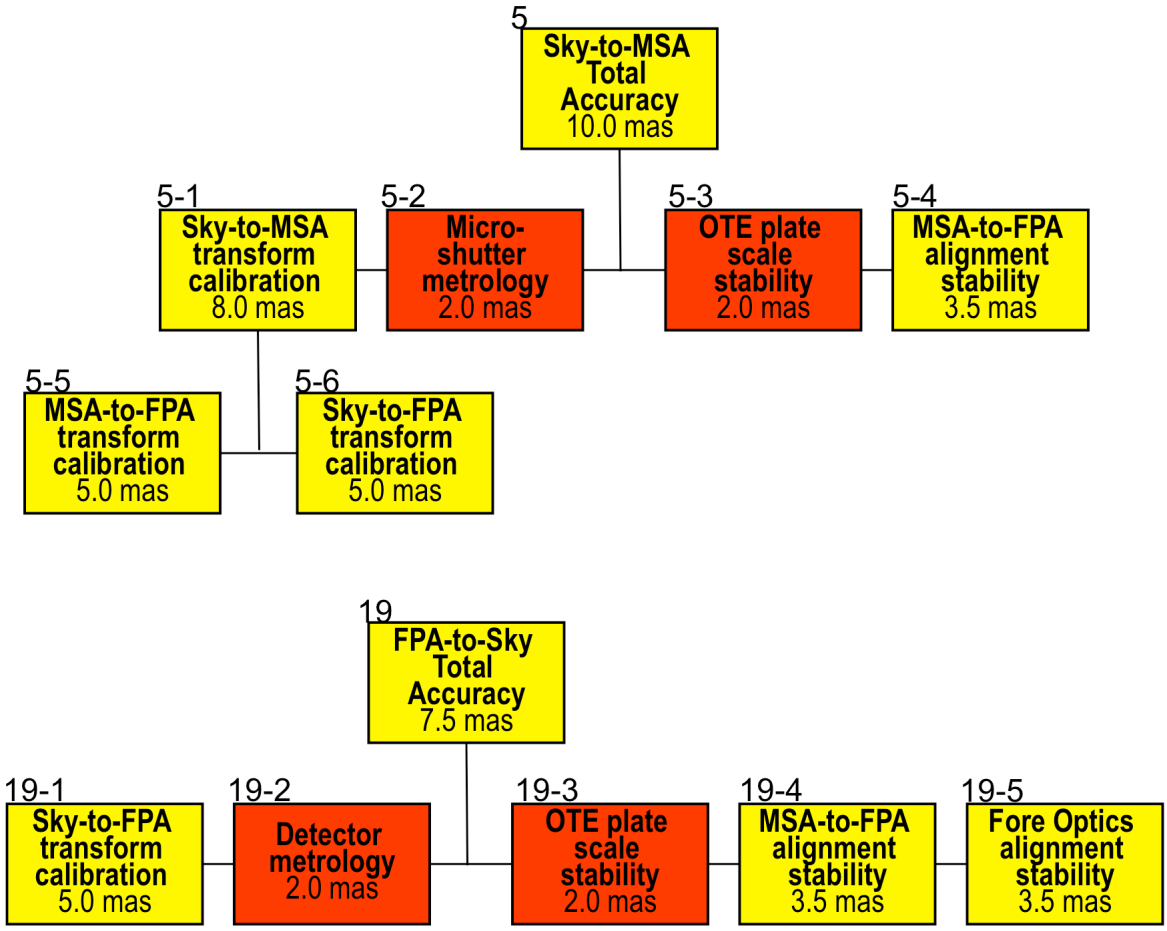

Figure 6. Graphical representation of the error budget for the NIRSpec target acquisition (from Böker 2008). Details for the Sky-to-MSA and FPA-to-Sky contributions shown in Figure 5.

As regards the other two components in the total error budget related to ESA-provided hardware (boxes 5 and 19 in Figure 5), at face value only the FPA-to-Sky transformation appears to depend explicitly on the repeatability of the GWA, while the Sky-to-MSA would seem to be independent of it, since the GWA is placed after the MSA in the optical train. However, since no detector is available at the MSA plane, also the Sky-to-MSA transformation depends on measurements done at the FPA plane and, therefore, also uncertainties in the GWA repeatability have to be considered. Figure 6 (from Böker 2008) offers a graphical representation of how the accuracies of the coordinate transformations between the image planes of Sky, MSA and FPA are interconnected.

The measurements described in Sections 2 and 3 allow us to characterise the accuracy achieved for several of the boxes shown in Figure 6, in particular, the accuracy of the MSA-to-FPA transformation (box 5-5; req. TA10 and R-178 in Table 1) and the stability of the alignment between MSA and FPA (boxes 5-4 and 19-4; req. TA9 and R-94 in Table 1). As shown in Section 2, our analysis indicates that the MSA-to-FPA transformation is very robust: we used the centres of half of the open micro-shutters in a checkerboard

configuration to predict the pixel positions of the other half, consistently finding residuals of 0.004 pixel (rms), or 0.4 mas. This value is derived from individual observations, involving no GWA reconfigurations, and as such it provides the intrinsic uncertainty of the transformation and compares very favourably with the allocated 5.0 mas (box 5-5; req. TA10 and R-177 in Table 1).

As for the stability of the MSA-to-FPA alignment, we can derive upper limits to it from the consistency of observations taken at different times. As shown in Table 2, the 20 observation sets used in this work were collected over a period 25 days, during which NIRSpec was used continuously, mimicking conditions of high in-orbit usage. The fact that the pixel offsets between the positions of the same micro-shutter in different observations have a residual of 2.5 mas (see Section 3), after correcting for the GWA movement, immediately indicates that the uncertainties in the MSA-to-FPA alignment stability must be less than 2.5 mas. Combining all contributions in quadrature, the 0.4 mas uncertainty on the MSA-to-FPA transformation (see Section 2) implies an uncertainty on the MSA-to-FPA stability of at most 2.4 mas in the extremely conservative assumption that the GWA sensors introduce no error. A more realistic assumption, in which the GWA sensor and the MSA-to-FPA stability have the same uncertainty, would give 1.7 mas for both. In either case, the values are comfortably within the allocated 3.5 mas (see boxes 5-4 and 19-4; req. TA9 and R-94 in Table 1).

Concerning the Sky-to-FPA transformation calibration (boxes 5-6 and 19-1; req. TA10 and R-179 in Table 1) and the alignment stability of the NIRSpec fore optics (box 19-5; req. TA8 and R-204 in Table 1), the analysis conducted by Gnata (2013) shows compliance with the required accuracy of, respectively, 5.0 mas and 3.5 mas. The remaining contributions to the total error budget in Figure 5 are not included in the system requirements that this section is meant to cover. Indeed, they come from uncertainties in the performance of NASA-provided hardware, namely the accuracy of the MSA and FPA metrology (boxes 5-2 and 19-2) and the stability of the plate scale at the focal plane at the entrance of NIRSpec (box 19-3). The latter component will only be verified once NIRSpec is installed on JWST and it will have to be confirmed in orbit, between and across the frequent re-phasing campaigns that the JWST primary mirror will undergo during the commissioning phase and standard operations. For now, we will therefore assume that the required 2.0 mas accuracy is met, since verification is not yet possible. On the other hand, upper limits on the accuracy of the MSA and FPA metrology can already be derived from the analysis presented in this work and we do so here, since our ultimate goal is to confirm the validity of the NIRSpec target acquisition approach.

As mentioned in Section 2, the only underlying assumption made in applying the method described by Giardino (2012) to derive the MSA-to-FPA and FPA-to-MSA transformations is that both the MSA and FPA have uniform and regular metrology across their faces. The fact that the fit residuals that we find in Section 3 are 2.5 mas implies that the combined contribution coming the MSA and FPA metrology must be certainly smaller than 2.5 mas. Therefore, considering all the other uncertainties contributing to the overall residuals, it is safe to conclude that the conditions set forth by boxes 5-2 and 19-2 are fully satisfied.

In summary, the values derived with the analysis illustrated in this section allow us to

conclude that the total Sky-to-MSA accuracy and the total FPA-to-Sky accuracy are well within the limits shown in Figure 6 (boxes 5 and 19; respectively reqs. TA10 and R-177 and TA10 and R-179 in Table 1), both for the dispersion and cross-dispersion directions. The actual derived values are 5.9 mas for the Sky-to-MSA transformation (box 5 in Figure 5), 3.5 mas or 4.8 mas, respectively in the dispersion and cross-dispersion directions, for the combination of filter correction and imaging mirror calibration (boxes 11 and 12 in Figure 5), and 6.5 mas for the FPA-to-Sky transformation (box 19 in Figure 5). Therefore, we can conclude that the overall contribution of ESA-provided NIRSpec hardware to the target acquisition uncertainty, as per the diagram in Figure 5, is well within the budget allocated to it in the NIRSpec System Requirements Document (Jensen 2013). Specifically, compliance with all the requirements listed in Table 1 is demonstrated. This guarantees that, as shown in the NIRSpec Target Acquisition Requirements (Böker 2008), with 5 reference stars it is possible to achieve an overall positioning accuracy better than 20 mas.

4.2 Compliance with the Functional Requirements Document

As mentioned above, the NIRSpec Functional Requirement Document (Smith 2008) demands that the target acquisition process place science targets in the respective micro shutters with an accuracy not exceeding 12.5 mas, both in the dispersion and cross-dispersion directions, with the use of no more than 20 reference stars (req. NSFR-37 in Table 1). Our measurements show that the good performance of ESA-provided NIRSpec hardware allows also this very stringent requirement to be met. We show this in Figure 7, which is identical to Figure 5 except for the fact that we have replaced the allocations on the uncertainty with the actual measured or derived values, indicated in underlined italics. The resulting total accuracy, assuming that 20 reference stars are used, is 11.6 mas in the dispersion direction (as shown in the figure) or 12.0 mas in the cross-dispersion direction. In both cases, the results are fully in line with requirement NSFR-37 in the NIRSpec Functional Requirement Document (Smith 2008), showing that the requested positioning accuracy is achievable.

5 SUMMARY AND CONCLUSIONS

In this work we have studied the performance of the position/tilt sensors installed on the imaging mirror mounted on the NIRSpec GWA, using MSA observations obtained during cycle 1 of the second NIRSpec flight model calibration campaign. The main purpose of this study is to analyse the impact of the GWA performance on the accuracy achievable with the NIRSpec target acquisition process. The most critical contribution of the GWA to the total target acquisition error budget is the accuracy with which a target of known coordinates can be placed within a preselected 200 mas wide micro-shutter, in spite of the limited rotational repeatability known to affect the GWA hardware. In order to overcome this known limitation, the GWA has been fitted with magneto-resistive sensors providing accurate knowledge of the actual GWA position. Therefore, it is crucial to characterise and calibrate the performance of the sensors and to assess any residual positional uncertainties associated with their use, particularly along the dispersion direction, which is the direction of primary scientific concern.

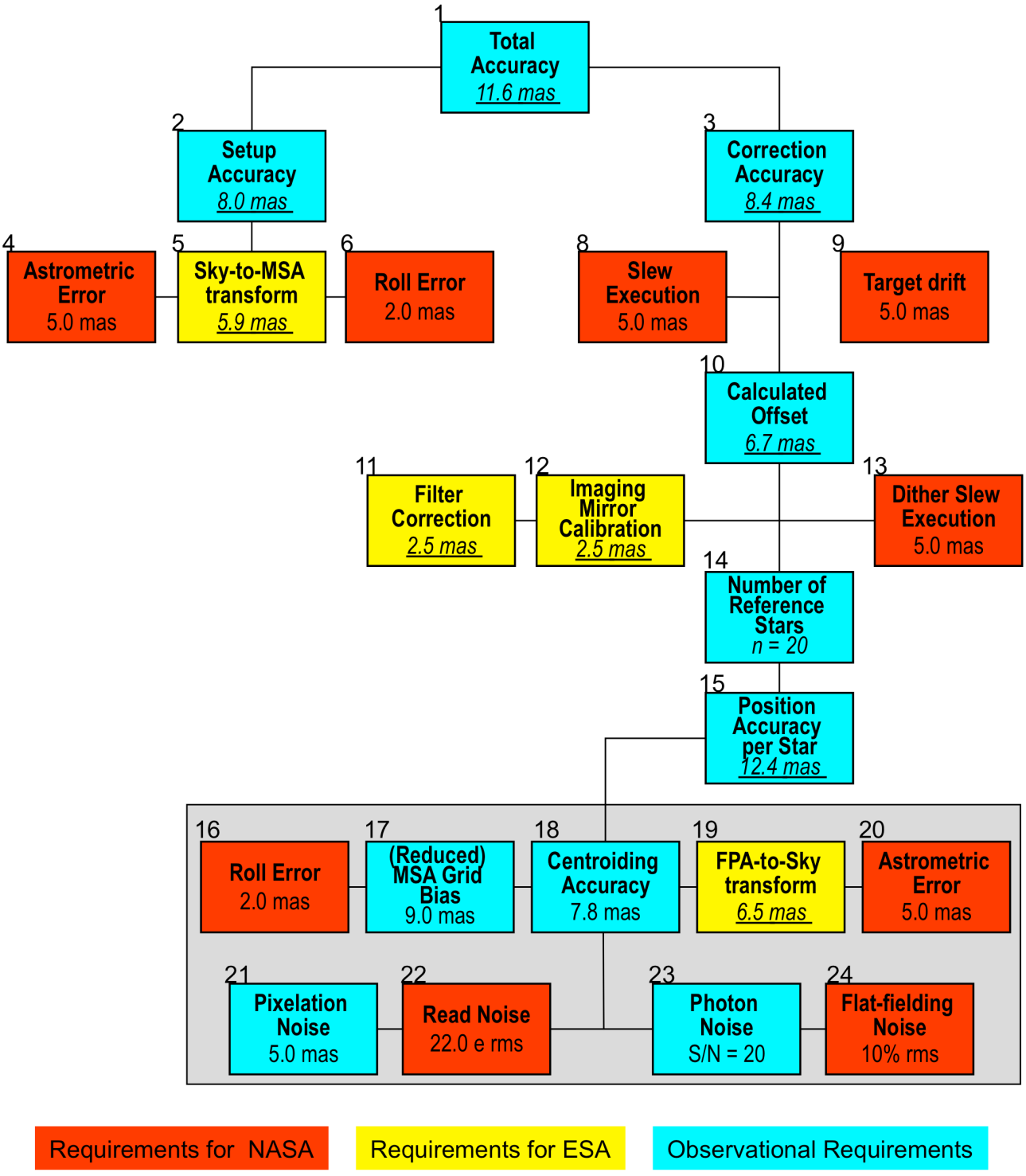

Figure 7. Same as Figure 5, but for the actually measured or derived values (in underlined italics).

Our analysis confirms the previously reported tight relationship between the sensors readings and the offset along the dispersion direction (De Marchi 2012a; De Marchi et al. 2012b). We show that this result is valid across the entire field of view, with a residual scatter of less than 2.5 mas (rms). This includes not only the uncertainties caused by the non-repeatability of the GWA mechanism, but also the uncertainties inherent in the MSA-to-FPA and FPA-to-MSA coordinate transformations and their temporal stability. Offsets

in the cross-dispersion direction are found to be marginal, typically less than 2.5 mas (rms), and never worse than 15 mas, so no correction is needed. We demonstrate that, within the stated 2.5 mas accuracy in the dispersion and cross-dispersion directions, we can accurately predict the position of any object in the field of view, using the telemetry readings from the GWA sensors. We also show that the offsets caused by the rotational non-repeatability of the GWA correspond to a bulk motion across the entire FOV. Therefore, we conclude that the MSA-to-FPA and FPA-to-MSA distortion solutions can be applied with equally small residuals to all MSA quadrants. This implies that, during the target acquisition process, the same set of transformations can be used by the on-board software for all objects, across the entire NIRSpec FOV.

The current baseline approach for target acquisition is to acquire short exposures with the internal continuum lamp in imaging mode, in order for the flight software to derive the actual orientation of the GWA mirror from the location of the fixed slit images on the detector. At the moment this approach remains unchanged, but if the levels of accuracy derived so far are consistently reached throughout the commissioning and early operations phase, as we expect, it will be possible to reduce the need for internal calibration exposures, thus saving both time and usage of NIRSpec's internal mechanisms, thereby increasing their lifetime.

Comparing the results of our analysis with the specific requirements levied on the NIRSpec target acquisition process by the NIRSpec Target Acquisition Requirements (Böker 2008) and, at higher level, by the NIRSpec Functional Requirements Document (Smith 2008), we convincingly show that the overall contribution of ESA-provided NIRSpec opto-mechanical hardware to the total target acquisition error falls well within the allocated budget. Our results lend strong support to the validity of the NIRSpec target acquisition concept as originally developed by Jakobsen (2004a).

REFERENCES

Alves de Oliveira, C., De Marchi, G. 2013, "Calibration of the GWA position sensors – Part II," NPR-2013-008 / ESA-JWST-RP-19657 (Madrid: ESAC)

Böker, T. 2008, "Target Acquisition Requirements," ESA-JWST-RQ-5071 and JWST-RQMT-006993 (Noordwijk: ESTEC)

De Marchi, G. 2012a, "Calibration of the GWA position sensors – Part I," NPR-2012-002 (Noordwijk: ESTEC)

De Marchi, G., Birkmann, S., Böker, T., Ferruit, P., Giardino, G., et al. 2012b, "Calibrating the position of images and spectra in the NIRSpec instrument for the James Webb Space Telescope," Proc. SPIE 8442-84423G

Giardino, G. 2012, "Documentation for MSA-detect tool," NTN-2012-004 (Noordwijk: ESTEC)

Gnata, X. 2005,"Evaluation of the impact of target acquisition accuract on the radiometric calibration of NIRSpec," CRAL-PJT-NIRS-TN-200503-03 (Lyon: CRAL)

Gnata, X. 2013, "FM calibration and verification report," NIRS-ASD-TR-0143 (Ottobrunn: EADS)

Jakobsen, P. 2004a, “The NIRSpec Target Acquisition Concept,” ESA-JWST-TN-650 (Noordwijk: ESTEC)

Jakobsen, P. 2004b, “NIRSpec Target Acquisition and the Micro Shutter Array,” ESA-JWST-AN-1060 (Noordwijk: ESTEC)

Jakobsen, P. 2005, “Error Budget for NIRSpec Target Acquisition,” ESA-JWST-AN-3032 (Noordwijk: ESTEC)

Jensen, P. 2013, “Near-Infrared Spectrograph System Requirements Document,” ESA-JWST-RQ-322 (Noordwijk: ESTEC)

Redman, K. 2010, “Metrology Report – James Webb Space Telescope Project – NIRSpec Detector Subsystem”, JWST-RPT-015170 (Greenbelt: GSFC)

Schwinger, S. 2010, “Micro Shutter Assembly Flight Alignment Metrology Report,” JWST-RPT-015799 (Greenbelt: GSFC)

Smith, M. 2008, “Near-Infrared Spectrograph Functional Requirements Document,” JWST-RQMT-002060 (Greenbelt: GSFC)